Journal of Alloys and Compounds 509 (2011) 2154–2159

Contents lists available at ScienceDirect

Journal of Alloys and Compounds

journal homepage: www.elsevier.com/locate/jallcom

# Structural and nano-composite features of $TiO_2$–$Al_2O_3$ powders prepared by sol–gel method

M.A. Ahmed*, M.F. Abdel-Messih

*Chemistry Department, Faculty of Science, Ain Shams University, Cairo, Egypt*

ARTICLE INFO

*Article history:*
Received 29 April 2010
Received in revised form 23 October 2010
Accepted 27 October 2010
Available online 4 November 2010

*Keywords:*
$Al_2O_3$–$TiO_2$ composites
Sol–gel
X-ray diffraction
Crystal structure
Microstructure of the samples

ABSTRACT

In this investigation titania–alumina nanocomposites containing various compositions of titania and alumina were successfully prepared by controlled sol–gel method in attempt to study the structure, nature of phases, particle size and morphology of the composite samples. The structural changes and phase analysis were monitored by XRD, FTIR and SEM where the surface area was estimated by BET analysis. The particle size of the composite samples is in nanometric dimensions (18–40 nm). The role of alumina content on the structural properties, phase transformation, surface area and particle size of titania was investigated. The resulting mixed oxides possess rutile phase at low alumina content (up to 20%) and anatase phase is predominant at high alumina content (40–90%). The XRD results reveal that the grain size of the mixed oxides is reduced upon increasing in the alumina content indicating that alumina can effectively prevent titania particles from further growing up in the process of calcination. This is confirmed by large increase in the specific surface area for the composite samples. In addition tialite ($Al_2TiO_5$) compound was detected in composites with high content of alumina.



## 1. Introduction

Nanoparticles and nanostructural materials have been considered an attractive family of materials over the last decades due to their novel properties that are not present in the bulk. The unique properties of nanomaterials result from the small sizes and large specific surface areas. The design and fabrication of the nanostructured materials have received considerable attention due to their interesting physical and chemical properties, and their potential applications in industry and technology.

Nanocrystalline titanium dioxide has a widespread range of new applications as important material in photocatalyst [1], solar cell [2], chemical and marine industries [3] and humidity sensors [4]. Alumina has numerous applications ranging from catalysis [5,6] to optics [7], electronics [8] and biomedicine [9,10]. Alumina and titania have been used interchangeably for many applications and each has individual drawbacks. Alumina suffers from a decrease in the activity for many applications and titania tends to have lower surface area and reduced thermal stability [11,12]. A systematic study of a mixture of these two oxides may provide materials with improved characteristics in which the shortfalls of the individual oxides are improved [11]. Such a mixture may broaden the range of applications available to this hybrid material. In addition, tialite ($Al_2TiO_5$) is used as a potential adsorbent in the decontamination of chemical warfare agents [13], in materials for aeronautical and automotive purposes [14], in orthopedic and dental implants [15] and in petroleum hydrotreatments [11]. A significant amount of attention has been given to make a suitable composition of titania–alumina system to improve the characteristic features of this nano mixed oxide. Ramirez et al. synthesized equimolar composition of titania–alumina supports using 'mixing' and 'impregnation' methods. By mixing titania and boehmite followed by calcination they observe the formation of Ti–O–Al, whereas by adding titanium alkoxide to alumina a separate titania structure grew on the alumina surface due to the alkoxide incorporation into the alumina pores [16]. Zilkov et al. report that a composite of titania–alumina nanoparticles synthesized from metal alkoxides in ionic liquids produce materials with significantly greater surface area (486 $m^2/g$) [17]. Recently, Galaviz Pérez et al. report that the crystalline structure and the surface morphology of the nanostructure $Al_2O_3$–$TiO_2$ composite were strongly dependent on the nature of precursor and annealed temperatures [18]. In a newly published paper, a titania–alumina mixed oxide support containing small amount of alumina shows high catalytic activity for propane conversion [19]. Abdel El All and Ali El-Shobaky indicate in a recent report that $TiO_2/Al_2O_3$ nano composite possesses high electric conductivity compared with the pure oxides [20]. The existence of 20% alumina improves the structural and textural properties of hierarchical macro-mesoporous powders of a mixed titania–alumina systems prepared by hydrothermal method using

* Corresponding author. Tel.: +20 224831836.
*E-mail address:* abdelhay71@hotmail.com (M.A. Ahmed).

0925-8388/$ – see front matter © 2010 Elsevier B.V. All rights reserved.
doi:10.1016/j.jallcom.2010.10.172

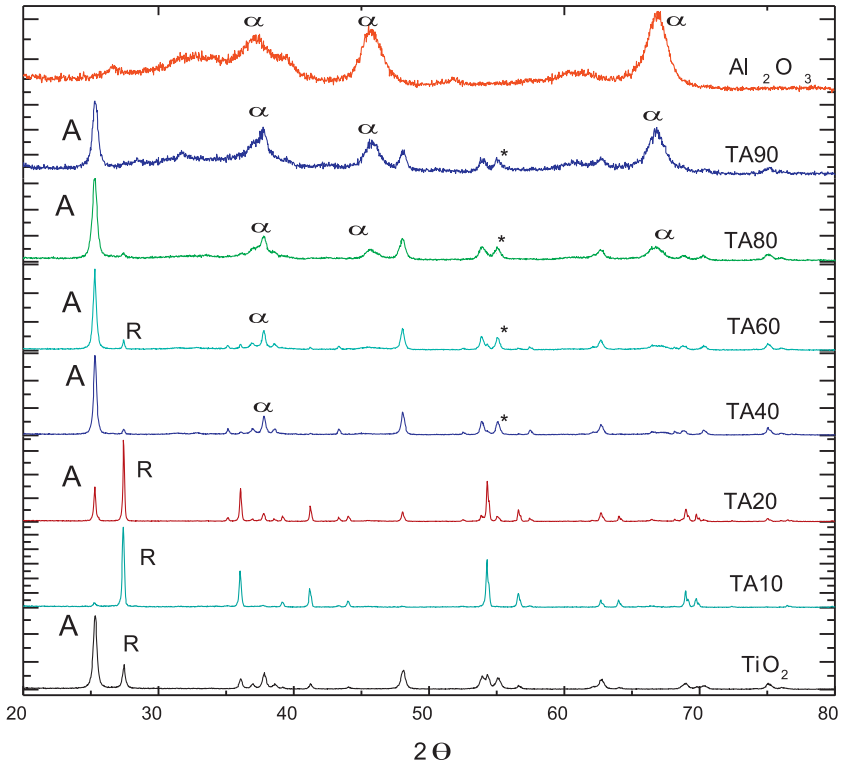


**Fig. 1.** X-ray diffraction of $TiO_2$, TA10, TA20, TA40, TA60, TA80, TA90 and $Al_2O_3$: (A) anatase-$TiO_2$, (R) rutile-$TiO_2$, (α) α-$Al_2O_3$ and (*) $Al_2TiO_5$.

tween-20 as structural surfactant directing agent [21]. In addition, doping alumina in the pore wall of titania improves the crystalline pattern and increases in the thermal stability of highly ordered mesoporous titania–alumina mixed oxide thin films [22]. Dejang et al. indicate the formation of $Al_2TiO_5$ in titania–alumina composites which contain various compositions of titania (0–20 wt%) prepared by plasma sprayed method [23].

In recent years, additional efforts have been devoted to the synthesis of $Al_2O_3$–$TiO_2$ nanocomposite architectures [24]. Thus, various synthesis methods have been employed to attempt well dispersed nanostructured composites such as sol–gel synthesis [25–27], hydrothermal synthesis [28], microwave-combustion synthesis [29], chemical vapor deposition [30], and spin coating method [31]. Among various methods, 'sol–gel' is of great interest since this method provides a great degree of control over molecular-scale mixing. Since this method is a solution process, it has all the advantages over other preparation techniques in terms of purity, homogeneity, felicity and flexibility in introducing dopants in large concentrations, stoichiometric control, ease of processing and composition control. Through sol–gel process, the growth of $TiO_2$ and $Al_2O_3$ particles can be effectively controlled by hydrolysis and condensation of titanium and aluminum salts in aqueous medium.

Most of the reports deal with the preparation of the titania–alumina nanocomposites using corresponding alkoxides and the resulting samples have small particle size and higher surface area, but these methods involve the use of alkoxides as starting materials which cost is relatively higher and the route of synthesis is more complicated.

Nevertheless there is a lack of systematic studies dealing with phase composition, particle size and microstructure of titania–alumina nanocomposites prepared by sol–gel method using simple and low cost metal salts precursors.

In the present study, we made an attempt to synthesize various compositions of titania–alumina nanocomposites ($x$ = 0, 10, 20, 40, 60, 80 and 100 wt% $Al_2O_3$) by controlled sol–gel method using simple salts of lower costs as metal chlorides. The structure, crystal phases, particle size, surface area and morphology of nanocomposites are investigated. In addition, the role of alumina on the phase transformation and microstructure of titania is reported.

## 2. Experimental

### 2.1. Materials

Aluminum chloride (Prolabo) and titanium chloride (Prolabo) were used as precursor for preparing high alumina–titania nanopowder. Solutions of aluminum chloride and titanium chloride were mixed together in the required proportions to yield different $TiO_2$–$xAl_2O_3$ (where $x$ = 0, 10, 20, 40, 60, 80, 90 and 100 wt%) batches. The mixed solutions were stabilized at room temperature and this temperature was kept throughout the experiment, together with continuous stirring. The mixed hydrogel was obtained by the drop wise addition of ammonium hydroxide solution into the continuously stirred mixed aqueous solution of Al and Ti salt and the viscosity of the batch gradually increased and finally set to an enblock gel at pH 7–8. The gels were then aged at room temperature for 48 h. Subsequently, the gel of each composition was washed repeatedly with distilled water to remove chloride ions and filtered. The filter cake was dried at 80 °C for 24 h. The dried gels were calcined in air in a muffle furnace at temperatures 900 °C with a hold time of 2 h at the corresponding peak temperatures. The composition of each batch has been listed in Table 1. The titania–alumina mixed oxides were labeled as TA$x$, where $x$ corresponding weight percent (wt%) of alumina.

**Table 1**
Phase composition (%) of anatase and rutile, particle size, surface area for $TiO_2$–$Al_2O_3$ composite samples.

| System | Titania phase composition (%) | | Particle size (nm) | | Surface area ($m^2$/g) |
|---|---|---|---|---|---|
| | Anatase | Rutile | Anatase | Rutile | |
| $TiO_2$ | 75 | 25 | 30.3 | 40 | 63.4 |
| TA10 | 4 | 96 | 29.8 | 38.3 | 70.3 |
| TA20 | 30 | 70 | 29.2 | 37.5 | 77.3 |
| TA40 | 94.4 | 5.6 | 24.3 | 37.2 | 94.6 |
| TA60 | 89.4 | 10.6 | 20.8 | 37.3 | 100.2 |
| TA80 | 94 | 5.6 | 18.6 | 36.5 | 123.5 |
| TA90 | ≈100 | Nil | 18.2 | Nil | 130.4 |

### 2.2. Material characterization

Fine and homogeneous powders of the different samples were back-loaded into the sample holder of a Philip Analytical X'PERT MPD diffractometer using CuKα radiation. The XRD patterns were recorded in a diffraction angle range from 20° to 100° with a step of 0.03° and integration time of 4 s per step. The diffraction patterns have been treated with the Rietveld refinement method using the MAUD program. The instrumental imperfections were evaluated with a sample of $LaB_6$ calibrated against a sample of NIST SRM-640b and provided by the Gem Dugout Company.

Fourier-transform infrared (FTIR) spectra were measured at room temperature on an ATT Mattson series FTIR TM spectrometer using the KBr disk technique.

Adsorption–desorption isotherms of purified $N_2$ at 77 K were determined using a conventional volumetric apparatus connected to a vacuum system that allowed prior outgassing to a residual pressure of $10^{-5}$ T.

The evolution of the morphology of the samples was examined by scanning microscopy (SEM) FE-SEM JEOL 6340.

## 3. Results and discussion

### 3.1. XRD structural analysis

The XRD patterns of titania, alumina and the mixed oxides samples are shown in Fig. 1. The crystal sizes of the samples were determined from the diffraction peak broadening using the Scherrer formula [32]. The anatase and rutile fractions of each sample were estimated from XRD intensity data using the Rietveld method of analysis [33] and the results are inserted in Table 1.

The XRD pattern of nano titania show several peaks at $2\theta = 25.3°$, 36.9°, 37.7°, 38.5°, 48°, 51.9°, 53.8°, 55.1°, 62.6°, 68.7° and 75° which are attributed to the anatase phase of titania in addition to some other peaks at $2\theta = 27.4°$, 39°, 41°, and 44° which are associated with the rutile phase. The diffraction peaks of the anatase phase are predominant which suggest that preparation of the oxide by sol–gel method stabilizes the anatase phase as the normal transformation of anatase to rutile form is usually occur at temperature range 500–800 °C. The XRD pattern of alumina represent several broad peaks with low intensity at $2\theta = 26.6°$, 31.3°, 36.9°, 39.5° and 51.8° which attributed to α-phase of alumina but the peaks indicate that the sample is in the early stage of crystallization.

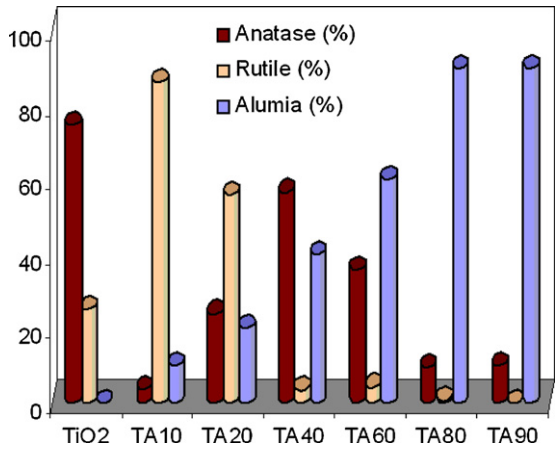


**Fig. 2.** Phase composition (%) of anatase and rutile crystallites of $TiO_2$, TA10, TA20, TA40, TA60, TA80 and TA90.

The diffraction patterns of the samples TA10 and TA20 indicate the predominant existence of the rutile phase of titania with very small peaks associated with the anatase phase, on the other hand the peaks observed for the other samples TA40, TA60, TA80 and TA90 are predominant which represent the anatase phase with a very small peaks associated with the rutile phase. It is interesting to remark that the amount of anatase crystallites in our samples increases with increasing alumina content (Fig. 2 and Table 1). Obviously the characteristic peaks corresponding to the different crystalline phases of alumina are completely missed in the samples which exhibit 10, 20 and 40% alumina compared with X-ray pattern of the pure oxide, the characteristic peaks of α-alumina start to appear in the sample containing 60% and increase in the

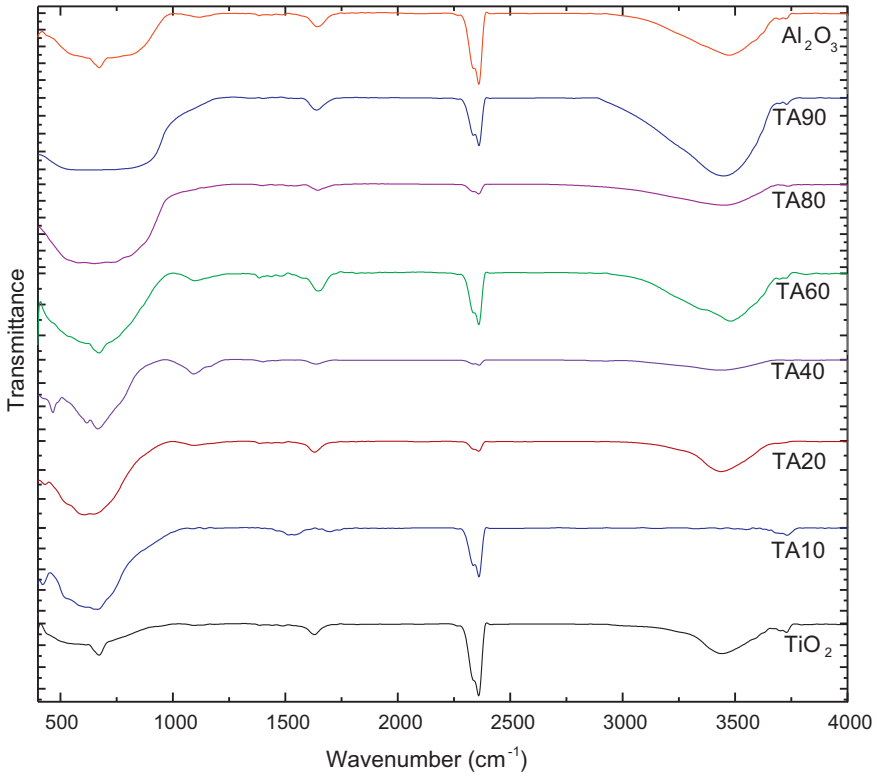


**Fig. 3.** FTIR of $TiO_2$, TA10, TA20, TA40, TA60, TA80, TA90 and $Al_2O_3$.

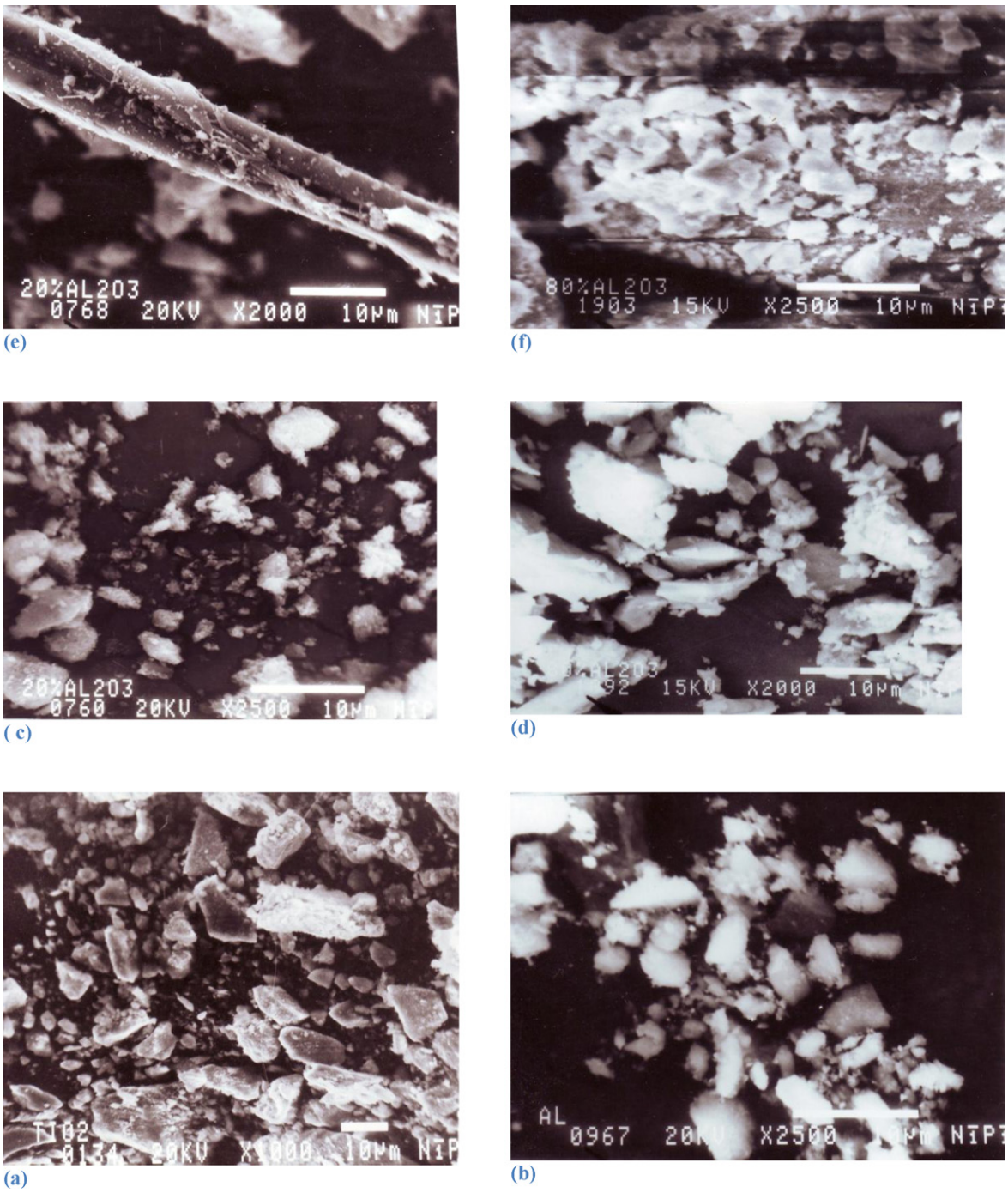


**Fig. 4.** SEM micrograph of (a) $TiO_2$, (b) $Al_2O_3$, (c) TA20, (d) TA80, (e) TA20, and (f) TA80.

samples with 80 and 90% alumina. The particle size of anatase and rutile phase is in the range of nano-scale (18–40 nm) and the addition of alumina shows a pronounced reduction in the crystallites size of titania as indicated in Table 1. In addition a remarkable peak broadening for the samples which possess high content of alumina is observed which implies the alumina can effectively inhibit $TiO_2$ crystallites from further growing up during the process of calcinations.

On examining Fig. 1, one can notice a characteristics peak for a tialite ($Al_2TiO_5$) compound in a sample TA40, TA60, TA80 and TA90. The XRD patterns provide evidence for the formation of tialite phases in the samples in which alumina is present in high content. This result is in agreement with work of Morris et al. [26] who indicate the formation of tialite in titania–alumina mixed oxides contain either excess of alumina or titania in composite samples.

There are three well-known $TiO_2$ crystalline types: anatase, rutile, and brookite. The anatase–rutile transformation temperature range varies from 673 K to 1473 K, depending on the method of synthesis, the atmosphere and the presence of foreign ions. The mechanism by which the additives either inhibit or promote anatase–rutile transformation has been related to the defect structure of the titania i.e., the concentration of oxygen vacancies or Ti interstitials. It was suggested that the additives which can increase the concentration of oxygen vacancies would tend to promote the

transformation, while some additives would retard the transformation by increasing the lattice defect concentration of Ti interstitials in titania [34–39].

It is clear from our results that nano alumina particles play a primordial role on the nature of phases and crystallites size of titania in composite samples. It is most probably that during the sol–gel process a homogenous mixture which contain Ti–O–Al bond is formed. By thermal treatment the mentioned bonds are broken and independent crystallization of the two oxides occurs. However, only titania is present in the XRD pattern because its tendency to crystallize is higher than that of alumina. Incorporation of some proportion of alumina into titania crystallites in TA10 and TA20 sample can be a suitable cause for acceleration the anatase-to-rutile transformation. The reason is that $Al^{3+}$ ions with a valence lower than $Ti^{4+}$ can substitute it and create oxygen vacancies due to the necessity of charge balance [21,40], thus the addition of this proportion of alumina favors the nucleation of rutile phase on the surface and spread their growth into $TiO_2$ particles. The composite samples containing high content of alumina (40–90%) are predominant possesses anatase phase of titania and α-phase of alumina. It is worth noting that TA60 sample which contains 60% alumina are predominant possesses anatase phase of titania and small peaks associated with α-phase of alumina. We can suppose that part of alumina is diffused on the surface grain boundary as a highly dispersed amorphous oxide coating the $TiO_2$ nanocrystallites and suppresses the grain growth of anatase and the other part segregates forming a separate α-alumina. This result is in agreement with some authors [37,39] who suggest that the presence of high content of alumina would prevent the nucleation of rutile by interfering the mutual contact of $TiO_2$ particles, so by this way some proportion of alumina prevents the small particles of titania from growing to a size necessary to allow the commencement of the transition into the stable rutile modification. In this way, a considerable proportion of alumina species may have been excluded from participation in the formation of alumina crystallites, thereby explaining the reduction in the intensity of diffraction peaks associated with the alumina modification.

### 3.2. Surface characterization

The specific surface area measurements of all samples are shown in Table 1. It is clear that increasing in the alumina content is accompanied by increase in the surface area of the composite samples as the role of alumina is to prevent the small particles from agglomeration and prevent the formation of large particles. This is confirmed from X-ray measurements by the large reduction in grain size on increasing in alumina content as indicated in Table 1. $Al_2O_3$ acts as a barrier against the advancement of grain boundaries of $TiO_2$ and effectively prevented the grain growth and loss in surface area.

### 3.3. FTIR spectra

FTIR is a very sensitive and well established tool for studying the orientation, transformation and nature of hydroxyl bonds in both alumina and titania hydrogel. The position and intensity of the IR peaks are strongly influenced by the crystallization behavior, degree of crystallinity, morphology and particle size. Therefore, the FTIR results could well be correlated with the crystallization behavior and phase evolution in titania–alumina composites.

Fig. 3 displays the FTIR spectra of titania–alumina nano composites. The spectrum of pure titania shows a large broad band at 3600–3400 $cm^{-1}$ that can be assigned to bridged OH modes (stretching modes). This band is in the hydroxyl stretching region and O–H vibration of the Ti–OH groups and surface adsorbed $H_2O$ molecules. The band around 3720 $cm^{-1}$ can be assigned to terminal O–H vibration of the Ti–OH groups [41]. The narrow band around 1600 $cm^{-1}$ can be assigned to OH (bending modes) of hydroxyl group and surface adsorbed water. In the low spectral region (400–1000 $cm^{-1}$), the band of a Ti–O–Ti bond of a titanium oxide network is detected at 640 $cm^{-1}$ [41].

The FTIR spectra of alumina show an intense band centered around 3447 $cm^{-1}$ and a broad band at 1640 $cm^{-1}$, which are assigned to stretching and bending modes of adsorbed water [42]. A small band at 1073 $cm^{-1}$ and a shoulder at 1163 $cm^{-1}$ are detected due to the symmetric and asymmetric bending modes of Al–O–Al bonds, respectively [42]. The OH torsional mode observed at 750 $cm^{-1}$ overlaps with Al–O stretching vibrations [42]. The band observed at 620 $cm^{-1}$ is attributed to stretching mode of $AlO_6$ [42]. The broad band in the region of 500–750 $cm^{-1}$ is assigned to α-$AlO_6$, whereas the shoulder at 890 $cm^{-1}$ is assigned to α-$AlO_4$ [42].

The FTIR spectra of the composite samples show a pronounced bands at 3400 and 1620 $cm^{-1}$ due to the hydroxyl group of the oxides and surface adsorbed water [41]. A broad band centered at 640 $cm^{-1}$ is detected which can assigned to Al–O–Al and Ti–O–Ti. In addition, a new small bands are detected at 583 and 439 $cm^{-1}$ which can be assigned to hetero metal–oxygen bonds of –Ti–O–Al–, these bands are more illustrated in the samples TA10 and TA20 [43] and are probably implying the incorporation of alumina into the framework of titania.

### 3.4. Scanning electron microscope

Fig. 4a–f depicts the microstructure of the pure and mixed oxides. The micrograph of titania shows that the material consists of two different types of pieces of partially crystallized gels of different sizes; one can be attributed to the anatase crystal and the other corresponds to the rutile phase. The micrograph of alumina indicates that a sample contains transparent gel particles of small size. The micrograph of a sample TA20 indicates that a material possesses both crystal of titania and transparent alumina particles but the titania particles are predominant and a pronounced reduction in particle size of the composite sample is detected, on the other hand a sample TA80 possesses titania and alumina particles but alumina particles are predominant. A characteristic rod is observed in Fig. 4e for the composite sample TA20 on which a small spherical particle is attached. On examining the micrograph of TA80, one can notice that the transparent alumina particles covered completely the titania gel which confirm the formation of alumina layers between titania particles that prevent the enlargement of titania crystallites and stabilize the anatase phase as discussed previous in XRD section.

## 4. Conclusions

Titania–alumina nanocomposites containing various compositions of titania and alumina were prepared by controlled sol–gel method using simple salts as$TiCl_4$ and $AlCl_3$ and all the composite samples are in nanometric dimension. Alumina plays a primordial role on the nature of crystalline phases, surface area and crystallite size of titania. Materials with up to 20% alumina possess a rutile phase while those with an excess of alumina exhibit only anatase crystalline phase of titania in addition to α-phase of alumina. The formation of tialite compound in the samples in which alumina is present in high content is detected. The transformation of anatase–rutile phase in the samples TA10 and TA20 can be explained by the incorporation of alumina in the crystal lattice of titania. The stabilization of the anatase phase in the samples possesses high content of alumina can be attributed to the formation of alumina layers between titania crystallites particles, alumina plays the role of a surfactant in preventing the small titania particles from agglomeration into large particle phase which is accompanied by decrease in particle size and increase in surface area.

## References


[1] A. Dodd, A. McKinley, T. Tsuzuki, M. Saunders, J. Alloys Compd. 489 (2010) L17–L21.
[2] L. Zhang, A.J. Xie, Y.H. Shen, S.K. Li, J. Alloys Compd. 505 (2010) 579–583.
[3] A.N. Alhazaa, T.I. Khan, J. Alloys Compd. 494 (2010) 351–358.
[4] L. Zheng, M. Xu, T. Xu, Sens. Actuators 66 (2000) 28–30.
[5] J. Cejka, Appl. Catal. A 254 (2003) 327–338.
[6] H.R. Zargar, M.R. Bayati, H.R. Rezaie, F.G. Fard, R. Molaei, S. Zanganeh, A. Kajbafvala, J. Alloys Compd. 507 (2010) 443–447.
[7] Y. Teng, Y. Zhuang, G. Lin, J. Zhou, B. Zhu, J. Qiu, J. Alloys Compd. 479 (2010) 378–381.
[8] S. Kurien, J. Mathew, S. Sebastian, S.N. Potty, K.C. George, Mater. Chem. Phys. 98 (2006) 470–476.
[9] S.E. Kim, J.H. Lim, S.C. Lee, S.-C. Nam, H.-G. Kang, J. Choi, Electrochim. Acta 53 (2008) 4846–4851.
[10] S. Iftekar, J. Grins, G. Svensson, J. Loof, T. Jarmar, G.A. Botton, C.M. Andrei, H.J. Engqvist, J. Eur. Ceram. Soc. 28 (2008) 747–756.
[11] H.K. Mishra, M. Stanciulescu, J.-P. Charland, J.F. Kelly, Appl. Surf. Sci. 254 (2008) 7098–7103.
[12] J. Choi, J. Kim, J.S. Yoo, T.G. Lee, Powder Technol. 181 (2008) 83–88.
[13] T.M. Zima, N.I. Baklanova, N.Z. Lyakhov, Inorg. Mater. 44 (2008) 146.
[14] F. Vaudry, S. Khodabandeh, M.E. Davis, Chem. Mater. 8 (1996) 1451–1464.
[15] V.R. Gonzalez, R. Zanella, G. de Angel, R. Gomeza, J. Mol. Catal. 281 (2008) 93–98.
[16] J. Ramirez, G. Macias, L. Cedeno, A. Gutierrez-Alejandre, R. Cuevas, P. Castillo, Catal. Today 98 (2004) 19–30.
[17] N. Zilkov, A. Zukal, J. Cejka, Micropor. Mesopor. Mater. 95 (2006) 176–179.
[18] J.A. Galaviz Pérez, J.A. Montes de Oca Valero, J.R. Vargas Garcia, H.J. Dorantes Rosales, J. Alloys Compd. 495 (2010) 617–619.
[19] D. Shee, G. Deo, A.M. Hirt, J. Catal. 273 (2010) 221–228.
[20] S. Abd El All, G. Ali El-Shobaky, J. Alloys Compd. 479 (2009) 91–96.
[21] M.L. Garcia-Benjumea, M.I. Espitia-Cabrerab, M.E. Contreras-Garciaa, Mater. Charact. 60 (2009) 1482–1488.
[22] H. Oveisi, A. Beitollahi, M. Imura, C.W. Wuc, Y. Yamauchi, Micropor. Mesopor. Mater. 134 (2010) 150–156.
[23] N. Dejang, A. Watcharapasorn, S. Wirojupatump, P. Niranatlumpong, S. Jiansirisomboon, Surf. Coat. Technol. 204 (2010) 1651–1657.
[24] G. Mouret, K. Mozet, H. Muhr, E. Plasari, M. Martin, Powder Technol. 190 (2009) 84–88.
[25] A. Bottino, A. Comite, G. Capannelli, Asia-Pac. J. Chem. Eng. 5 (2010) 242–248.
[26] S.M. Morris, J.A. Horton, M. Jaroniec, Micropor. Mesopor. Mater. 128 (2010) 180–186.
[27] S. Abd El All, G.A. El-Shobaky, J. Alloys Compd. 479 (2009) 91–96.
[28] M.L. García-Benjume, M.I. Espitia-Cabrera, M.E. Contreras-García, Mater. Charact. 60 (2009) 1482–1488.
[29] G. Golkar, S.M. Zebarjad, J.V. Khaki, J. Alloys Compd. 504 (2010) 566–572.
[30] Z. Yanqing, S. Zhizhan, L. Wenjun, H. Xingfang, J. Mater. Chem. 11 (2001) 1547–1551.
[31] M. Wang, H. Lin, T. Yang, J. Alloys Compd. 473 (2009) 394–400.
[32] B.D. Cullity, Elements of X-ray Diffraction, Addison-Wesley Publishing Company, Inc, London, 1978, p. 99.
[33] L. Lutterotti, Maud 2.044, http://www.mg.unitn.it/~Luttero/maud.
[34] Y. Jung, D. Kim, Y. Kim, E. Park, S. Baeck, J. Phys. Chem. Solids 69 (2008) 1464–1467.
[35] R.A. Eppler, J. Am. Ceram. Soc. 70 (1987) 64.
[36] X.Z. Ding, X.H. Liu, Y.Z. He, J. Mater. Sci. Lett. 13 (1994) 462.
[37] W. Zhiyi Wang, D. Deng, Mater. Sci. Eng. B 140 (2007) 109–113.
[38] R. Rodriguez, S. Vargas, R. Arroyo, R. Montiel, E. Haro, J. Mater. Res. 12 (1997) 439.
[39] H. Oveisi, A. Beitollahi, M. Imura, C. Wu, Y. Yamauchi, Micropor. Mesopor. Mater. 134 (2010) 150–156.
[40] S. Borkar1, S. Dharwadkar, J. Therm. Anal. Calorim. 78 (2004) 761.
[41] M.J. Velasco, F. Rubio, J.L. Rubio, Thermochim. Acta 326 (1999) 91–97.
[42] G. Urretavizcaya, A.L. Cavalieri, J.M. Porto Lopez, I. Sobrados, J. Sanz, J. Mater. Synth. Process. 6 (1998) 1–7.
[43] S. Tursiloadi, H. Imai, H. Hirasima, J. Non-Cryst. Solids 350 (2004) 271–276.